解説

Dynamics of Inner Shell Resonant Raman Scattering

Hans ÅGREN[1], Faris GEL'MUKHANOV[2] and Pawel SALEK[1]

[1*]*Theoretical Chemistry, Royal Institute of Technology*
[2]*Institute of Automation and Electrometry*

Some recent advances in the theory of the resonant Raman process for atoms, molecules and solids involving inner shell electrons are reviewed. Special emphasis is put on the dynamical aspects and on the notion of a duration time for the x-ray Raman process (RXS), which brings about a distinction of processes with different time scales responsible for the formation of the spectral profile. This notion has been useful for actual predictions of various phenomena associated with RXS such as "symmetry restoration", "vibrational collapse", and "control of dissociation". The temporal theory of RXS is based on the wave packet formalism. The increase of the broad "molecular" parts relative to the atomic, or fragment, decay upon frequency detuning is demonstrated. The atomic-like resonance and molecular parts are proved to show different dispersion relations. Under certain conditions the interference between the molecular and atomic parts produces conspicuous "spectral holes". These conceptual tools are applicable also in the case of solids; there is an analogous restoration of momentum selection rules and a collapse effect upon detuning the frequency. Thus when the duration of the scattering is shortened by a large detuning, the role of electron-phonon coupling of the core excited states is suppressed. The shortening of the RXS duration in a certain sense leads to a delocalization of the core hole in a solid. We describe also some new features that derive from the Doppler effect on ejected Auger electrons.

1. Introduction

Contemporary experiments in the x-ray region using synchrotron radiation sources are stationary, and the many new phenomena obtained in synchrotron laboratories have therefore up to this time received interpretations mostly by means of time-independent theory[1-3]. However, even if time-dependent interpretations do not follow naturally from the experiment, and even if they principally do not provide new information compared to the time-independent ones, they have recently gained increased popularity owing to their inherent interpretability and our inclination to relate spectral features to processes rather than to states.

One of the important characteristics of the dynamics of a resonant x-ray Raman scattering process is the "duration time"[2,4-8], which presents a pure quantum notion based on the interference, or dephasing, suppression of large time contributions to a scattering amplitude. This notion has provided a deeper insight into the formation of the RXS spectral profile[5,7-12]. With the variation of the duration time through detuning the energy one can monitor and even control different microscopic dynamical processes responsible for the RXS spectral shape. Thus central concepts as symmetry and momentum selectivity, the formation of band profiles and the competition between dissociation and decay, have been shown to possess truly "dynamic" features in that they depend on both excitation frequency and on lifetime broadening- and therefore on the RXS duration.

The notion of a duration time is also associated with some profound contradictions[13]: For example, to reach the fast limit for the RXS amplitude (short duration of RXS) the wave packet evolution must exceed the lifetime by several times. The RXS duration can be presented as a complex quantity, with the real and imaginary parts responsible for the irreversible decay and reversible dephasing processes, respectively. It also provides a counterintuitive relation between the time of the evolution of the wave packet at the core excited state and the duration time of the scattering process. The effective duration of RXS strongly depends on the detuning of the frequency of incident radiation from the photoabsorption band, while the relaxation time of the wave packet does not, but is instead characterized by the time of flight and the lifetime of the core excited state, both of which can considerably exceed the RXS duration time. The concept of the RXS duration can thus be applied directly only to the RXS process with the "time of measurements" larger than the lifetime of a core excited state[13].

The time dependent representation for the scattering amplitude allows to make a direct connection between the RXS amplitude and the RXS duration. Special emphasis is paid on cases when the core excited states are dissociative with spectral features containing both so-called atomic-like (AL)

* Theoretical Chemistry, Royal Institute of Technology, S10044, Stockholm, Sweden
TEL (+46)13 28 12 86 FAX (+46)13 13 75 68 e-mail agren@ifm.lie.se

resonances[4,14] and "molecular" backgrounds[4]. It is shown that the interference between these two contributions give rise to new, and quite unexpected, effects. Also the mapping effect of the wave packet and the interatomic potentials, proposed in ref. 4, 15, is a "useful" aspect of the wave packet theory. This mapping has been used to reproduce the square of the vibrational wave function of core excited state in very recent resonant Auger experiments[16].

We further review aspects of the space distribution of the wave packet and the role of the excitation energy on this space distribution, which also is of particular consequence for the interpretation of the resonant x-ray scattering experiment. We also shortly go through the theory for Doppler effects, which emerge as interesting spectral features associated with x-ray Raman scattering involving dissociative potential surfaces and AL resonances. It was predicted that the spectral shape of these AL resonances are strongly influenced by the Doppler effect for the ejected Auger electrons[17], something that was recently experimentally confirmed in resonant Auger spectra of O_2[18].

The time-dependent approaches are of importance also for interpreting RXS of solids and polymers, especially in cases with phonon coupling and momentum exchange between electrons and photons. Electron-phonon coupling is probably more the rule than the exception due to the degeneracy of the core shells which often leads to strong vibronic mixing of the core excited states with different symmetries. This may result in a violation of the electronic selection rules for the scattering process[9]. Such effects are most easily analyzed for π-electron polymers, for which analytical solutions of the phonon coupling problem can be achieved[19]. The electronic selection rules (in particular the momentum conservation law) are restored when the RXS duration is shorter than the period of vibrations and when the photon momenta are neglected, something that takes place for large detuning and short duration times of the RXS process[5,19-21]. The detuning thus quenches the electron-phonon interaction in the core excited state and leads to a narrowing (collapse) of the electron-vibrational bands both in molecules and solids[6,7,19]. So the electron-phonon interaction in x-ray Raman spectra is strongly dynamic, and the shortening of the duration time through frequency detuning allows an active manipulation of the strength of the electron-phonon interaction.

The present review is a written account and an elaboration of the talk given by one of the authors (H.Å) at the 1999 year meeting of the Japanese society for synchrotron radiation research held in Tsukuba 7-9 January 1999. For the basic mathematical formulations of the theories we refer to four publications that are central to this review;[13,15,17,19].

2. Duration Time

The time-dependent representation for the scattering amplitude is simply obtained as[13]

$$F=F(\infty),\ F(\tau)=-i\langle f\,|\,\Psi_T(\tau)\rangle=\int_0^\tau dt\,\mathscr{F}(t). \qquad (1)$$

where the wave packet $\Psi_T(\tau)$ describes all photoabsorption-decay paths up to the time τ and the amplitude $F(\tau)$ of all decay events up to this time; $\mathscr{F}(t)=-i\langle Q\,|\,\psi(t)\rangle\exp(-t/T)$. In a stationary experiment the RXS cross section collects all the decay events up to $\tau=\infty$. Here

$$|\Psi_T(\tau)\rangle=\int_0^\tau dt\,e^{-t/T}\,Q\,|\,\psi(t)\rangle,$$
$$|\psi(t)\rangle=e^{-i\mathscr{H}t}\mathscr{D}\,|\,o\rangle \quad \mathscr{H}=H_c-\bar{E}, \qquad (2)$$

H is the molecular Hamiltonian, and $\bar{E}$ is the average energy of a core excited state. Atomic units are used unless otherwise stated. We note that $|\psi(t)\rangle$, $|\Psi_T(\tau)\rangle$, and $F(\tau)$ can not be measured in current stationary RXS experiments due to the small intensity of the x-ray beam and the insufficient time resolution. Fast measurements would in principle allow to find the squared wave packet $|\psi(t)|^2$. One can measure this squared wave packet as well as $|\Psi_T(\tau)|^2$ (and $|F(\tau)|^2$) if the signals in the time domain $0\le t\le\tau$ are collected. The wave packet $|\Psi_T(\infty)\rangle$ and stationary RXS amplitude $F=F(\infty)$ correspond to measurements for a long duration time ($\tau\gg\Gamma^{-1}$) or to the ordinary stationary RXS experiments.

A. Complex duration time: Decay and dephasing times

The complex time

$$T=T_\Gamma+iT_\Omega=\frac{1}{\Gamma-i\Omega}=\tau_c e^{i\varphi},$$
$$\tan\varphi=\frac{\Omega}{\Gamma},\quad \tau_c=\frac{1}{\sqrt{\Omega^2+\Gamma^2}} \qquad (3)$$

characterizes the time scale of the RXS process, and can be referred to as a duration time of the scattering process. $\Omega=\omega-\bar{\omega}$ is defined here as the detuning of ω relative to the characteristic frequency $\bar{\omega}=\bar{E}-E_0$ of the x-ray absorption band.

The duration time is complex and consists of two different contributions[13]

$$T_\Gamma=\frac{\Gamma}{\Omega^2+\Gamma^2},\quad T_\Omega=\frac{\Omega}{\Omega^2+\Gamma^2}. \qquad (4)$$

The real, T_Γ, and imaginary, T_Ω, parts of the RXS duration time refer to the irreversible and reversible contributions, respectively, and depend differently on the detuning and the lifetime broadening Γ. Indeed, the dephasing is a reversible process contrary to the decay which is irreversible. T_Ω originates mainly from detuning and can be named as the "dephasing time" due to that contributions to the scattering amplitude interfere destructively owing to the phase difference $\Omega(t_2-t_1)$. This destructive interference suppresses the long-time contribution to the scattering amplitude if detuning is large and if a damping Γ exists. Only decay transitions in the time domain $0<t<|T|$ contribute significantly to F.

To put the subject of the RXS duration in a proper perspective, we give a qualitative discussion of this duration time for large detunings which results in fast oscillations of

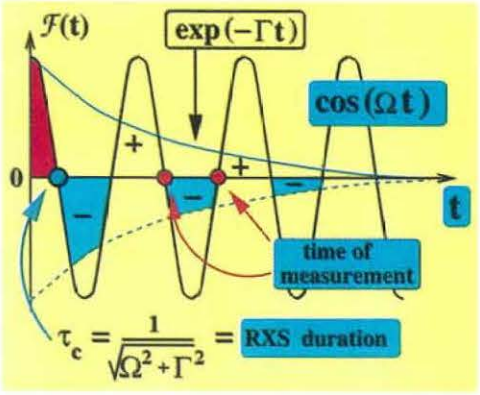

Figure 1. Formation of the scattering amplitude $F(\tau)=\int_0^\tau dt\mathcal{F}(t)$ (1) in short and long time domains. The case of 3-level system (ground, core excited, and final states). The fast oscillations with the frequency equal to Ω cancel each other only for long times of "measurement" $t\gg 1/\Gamma$. This results in the limit of the fast RXS. For smaller times, $t<1/\Gamma$, this cancellation is not complete.

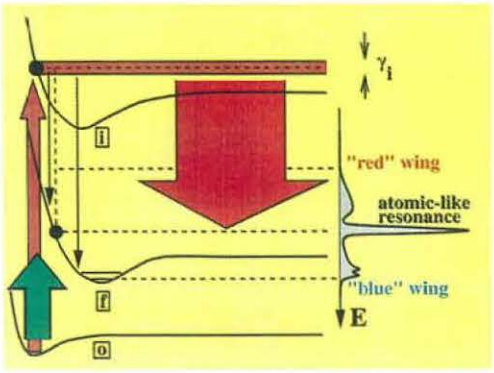

Figure 2. Formation of the atomik-like resonance with "blue" and "red" wings.

$\mathcal{F}(t)$ (1). **Fig. 1** shows that these fast oscillations ("+" and "−" domains) with the detuning frequency Ω cancel each other only for large times $\tau\gg 1/\Gamma$. In such a case only small time intervals (shorter than the RXS duration $t\lesssim\tau_c$) contributes to the scattering amplitude $F(\tau)$. For time intervals shorter than the lifetime broadening, $\tau\lesssim 1/\Gamma$, the cancellation of "+" and "−" regions is not complete and the times, $0\lesssim t\lesssim\tau$, give comparable contributions to $F(\tau)$ (1). **Fig. 1** explains the somewhat paradoxical situation that the fast limit for the RXS amplitude is obtained only when $\mathcal{F}(t)$ can go through the long time evolution (longer than Γ^{-1}). This fact reflects the qualitative distinction between the RXS duration time and the characteristic time Γ^{-1} of the wave packet evolution, something that is related to the interference of the intermediate core excited states. The destructive interference in the time domain stresses the quantum nature of the notion of the RXS duration.

One can see from **Fig. 1** that time-resolved RXS measurements make it possible to obtain stronger signals than in the stationary RXS experiment[13]. It should be mentioned that the more exact definitions of the duration time as "mean" or "average" times of the scattering imply strong asymmetry of the RXS duration as a function of the detuning[13].

B. Formation of space distributions of wave packets

Decay channels with dissociation preceding electronic decay were first identified more than 10 years ago, in measurements of HBr by P. Morin and I. Nenner[22]. These channels as well as core excitation above the dissociation threshold lead to AL narrow resonances in the spectra[4,8,14]. A qualitative picture of the formation of AL resonances with broad short- and long-wave wings[4,8,10,15] is given in **Fig. 2**. We remind that the AL resonances are caused by decay transitions in one of the fragments of the dissociation. If this fragment is an atom one observes AL single line resonances, **Fig. 2**. It is natural to attribute the notions "molecular band" or "molecular contribution" to the red and blue wings of the AL resonance since they are formed by decay transitions close to the equilibrium geometry of the molecule. In general, the RXS amplitude will be the sum of AL and molecular contributions[4]

$$F=F_{at}+F_{mol}. \tag{5}$$

The AL contribution has a spectral shape close to a Lorentzian[4,14]

$$F_{at}\propto\frac{1}{E-\omega_{cf}(\infty)+i\Gamma},\quad \omega_{cf}(\infty)=U_c(\infty)-U_f(\infty). \tag{6}$$

Here E is the energy of the emitted particle (x-ray photon or Auger electron). One can see that contrary to the dispersion law for the molecular contribution[23] the position of the AL resonance does not depend on the excitation energy[4,14]

$$E=\omega_{cf}(\infty). \tag{7}$$

It is illustrative to consider the space distribution of wave packets as a function of detuning and duration time. There is a principal distinction between the wave packet evolution for core excitation below and above the dissociation threshold. **Fig. 3** shows the space distribution for the bound core excited state $^1\Pi_u$ of N_2 for three different detuning energies. As clearly seen in this figure the contribution of the region outside of the ground state vibrational wave function is suppressed when the detuning is large (short τ_c). Indeed, due to the fast RXS a "direct" transition from the ground to the final nuclear state takes place[2,4]

$$F\simeq F_{mol}\propto\frac{\langle f|o\rangle}{\Omega+i\Gamma},\quad \tau_c\ll\tau_{vib},\ \tau_f, \tag{8}$$

where $\langle f|o\rangle$ is the Frank-Condon (FC) factor between vibrational wave functions of final and ground states, τ_{vib} and τ_f are the period of vibrations and time of flight, respectively; $\Omega=\omega-\omega_{co}$, $\omega_{co}=U_c(\infty)-U_0(R_0)-\omega_o/2$; $U_j(R)$ is the internuclear potential of electronic state j. This general result shows that in the fast limit only the "molecular" part,

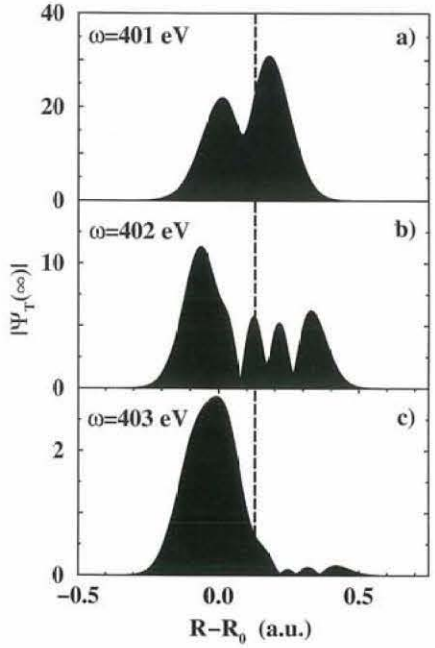

Figure 3. The space distribution of $|\Psi_T(\infty)|$ versus the RXS duration (detuning) for the bound core excited state $^1\Pi_u$ of N_2[13]. The contribution of the region outside of the ground state vibrational wave function is suppressed when Ω is large. Γ=0.065 eV. The RXS durations are: $|T| \simeq 5.6$ fs, 0.73 fs, and 0.35 fs for the excitation frequencies ω=401 eV, 402 eV, and 403 eV, respectively.

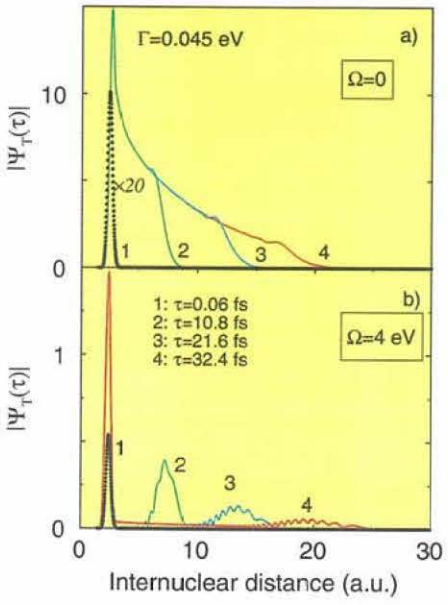

Figure 4. Time evolution of the absolute value of the wave packet $\Psi_T(\tau)$ (2) for different excitation energies[13]. The shape of the wave packet behind the wave front does not change. Cl L ($2p^{-1}\sigma^*$) dissociative core excited state in the HCl molecule. Γ=0.045 eV. a) Ω=0 eV, $|T| \simeq 14.6$ fs. b) Ω=4 eV, $|T| \simeq 0.16$ fs.

F_{mol}, contributes to the RXS amplitude since the nuclear subsystem in the core excited state has no time to vibrate and to change equilibrium geometry. Another profound aspect of eq. (8) is that the intensity of the AL peak is close to zero when the RXS duration τ_c is short[2,4,8].

Fig. 4 demonstrates the principal distinction between wave packet evolutions in bound and unbound potentials[13]. The wave packet evolves in one direction in a dissociative potential, in contrast to a bound potential where it moves back and forth periodically. One can see also that the space shape of the wave packet behind its front does not depend on time, and that the amplitude of the flat dissociative contribution to the wave packet is suppressed when the RXS duration decreases. This suppression takes place even for a lifetime broadening that goes to zero, an effect which is absent for discrete vibrational states where the space distribution of the wave packet oscillates without damping.

We see that when the wave front has left the molecular region, only the intensity of the AL peak changes with time. The wave front propagates for an infinitely long time when Γ=0, which results in a continuous increase of the intensity for the AL peak.

C. Time dependent representation for the RXS cross section

The above results demonstrate that the temporal language allows a deeper insight into the physics of x-ray scattering. The time-dependent representation is profitable also from the computational point of view. The RXS cross section can be evaluated for arbitrary spectral distribution of incoming radiation $\Phi(\omega-\omega_1, \gamma)$ with the width γ as the convolution [11,12,15,24]

$$\sigma(E, \omega)=\int d\omega_1 \sigma_0(E, \omega_1)\Phi(\omega-\omega_1, \gamma),$$
$$\sigma_0(E, \omega)=\frac{1}{\pi}\mathcal{R}e\int_0^\infty d\tau \sigma_0(\tau)e^{i(\omega-E+E_o)\tau}. \quad (9)$$

This reduces our problem to an evaluation of the RXS cross section for monochromatic excitation $\sigma_o(E, \omega)$ which can be found in terms of the autocorrelation function[4,15]

$$\sigma_o(\tau)=\langle\Psi(0)|\Psi(\tau)\rangle, \quad |\Psi(\tau)\rangle=e^{-iH_f\tau}|\Psi(0)\rangle,$$
$$|\Psi(0)\rangle=|\Psi_T(\infty)\rangle. \quad (10)$$

The solution is obtained in two steps; 1) the solution of the Schrödinger equation in the core excited state $i(\partial/\partial t)|\psi_c(t)\rangle = H_c|\psi_c(t)\rangle$ for $|\psi_c(t)\rangle=\exp(-iH_c t)\mathcal{D}|o\rangle$ with the initial condition $|\psi_c(0)\rangle=\mathcal{D}|o\rangle$, and 2) the solution of the Schrödinger equation for $|\Psi(\tau)\rangle$ with the final state Hamiltonian H_f and with the initial condition $|\Psi(0)\rangle$. Other time-dependent techniques for evaluations of the RXS cross section can be found in ref. 15.

3. Dynamical Wave Packet Calculations

The resonant Auger spectrum of HCl[8] has perhaps served as the best demonstration case for "dissociation before decay" in x-ray Raman scattering and is also a good candidate for applications of the theoretical algorithms briefly discussed in the foregoing. Cl 2p core excitation to the σ^* level

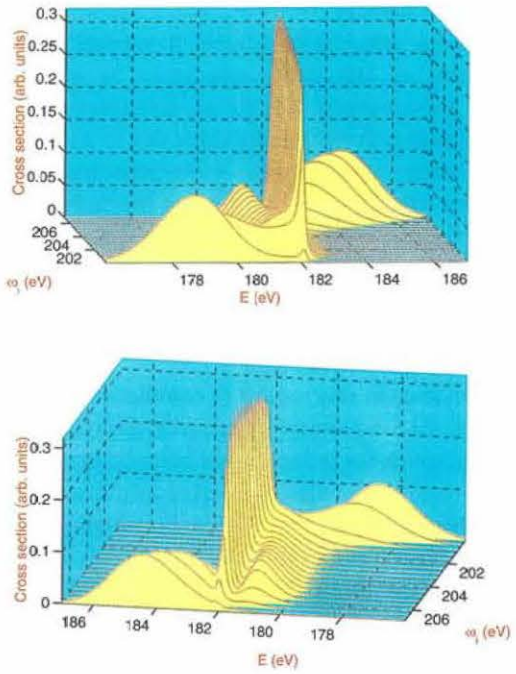

Figure 5. The RXS cross section for the unbound $^2\Sigma^-$ final state of HCl for different excitation energies. The RXS cross sections are normalized; the integral cross sections are the same for different excitation energies. $\gamma=0$[15].

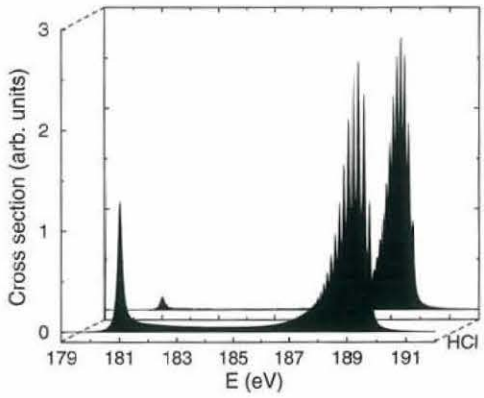

Figure 6. Isotope effect. Comparison of the RXS profiles for HCl and DCl. The bound final state is $^2\Sigma^+$, the detuning $\Omega=3$ eV and the lifetime broadening is $\Gamma=0.045$ eV.

leads to a dissociative potential on which the molecule can fragmentize before it decays[8]. Three final states can be singled out as representing the important states in the formation of the total spectrum: a $^4\Pi$, a $^2\Sigma^+$ and a $^2\Sigma^-$ state of HCl^+. All of them produce AL lines due to dissociation, the $^2\Sigma^+$ state also some structure due to a bound part of the potential. The molecular bands can origin from both the short-wave ($^2\Sigma^+$) or the long-wave ($^2\Sigma^-$, $^4\Pi$) sides of the AL resonance[15]. The AL resonance for the same final state can in general simultaneously have both blue and red tails[4,17], **Figs. 2** and **5**. The spectral shape of the molecular band strongly depends on the shape of the potentials. If the final

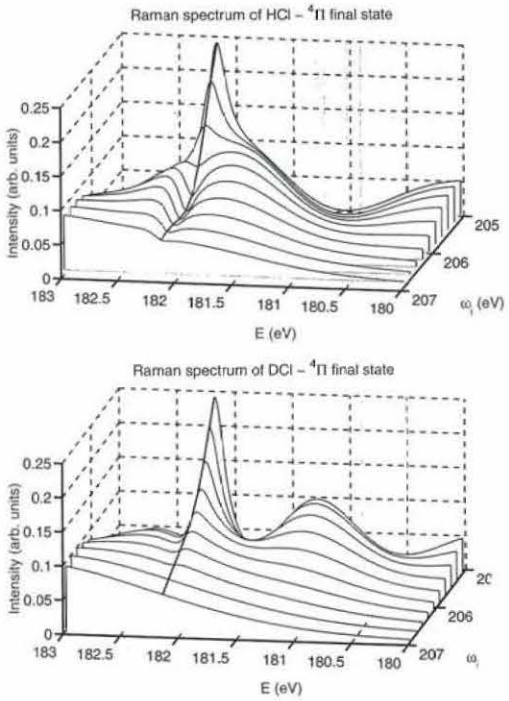

Figure 7. Isotopic effect. The RXS cross section for the unbound $^4\Pi$ final state of HCl and DCl. The dip ine HCl spectra is absent for DCl.

(or core excited) state is bound the molecular contribution consists of a vibrational band and a smooth continuum-continuum tail (**Fig. 6**).

The fine structure of the molecular contribution can also be understood with help of the reflection approximation in which the RXS spectral profile maps the space distribution of the wave packet[4,15] Additional fine structure in the RXS profile is caused by the inhomogeneous space distribution of the core excited wave packet $|\Psi(0)\rangle$ in the molecular region (see **Fig. 5**).

The limit of fast RXS is reached for quite large $|\Omega|$. The simulations show that the RXS profile begins to copy the photoabsorption profile (**Fig. 5**) of the $o\rightarrow f$ direct transition only when $\Omega\lesssim -3$ eV or when $\Omega\gtrsim 4$ eV. One can see that the intensity of the AL profile tends to zero in this limit in accordance with equation (8).

Fig. 7 demonstrates the appearance of a striking spectral feature of the RXS profile when the narrow AL resonance is embedded in the smooth molecular background, namely that the AL resonance converts into a spectral hole when the frequency is tuned from the photoabsorption resonance. This is the result of an interference between the broad molecular background (8) and the narrow AL resonance (6)[15]. The "hole" disappears for large detunings where the RXS profile coincides with the photoabsorption band of the direct $o\rightarrow f$ transition (see lower panel in **Fig. 7**). Contrary to a naive picture, the narrow spectral hole is not blurred when the width γ of the incident radiation increases. The simulations[15] demonstrate that the hole can even be trans-

formed into a peak when γ increases. **Fig. 7** shows that the spectral dip disappears going from the HCl to the DCl isotopomers.

Apparently the dynamics of the formation of the RXS profile depends on both the RXS duration τ_c (3) and the internal characteristic times of nuclear motion (like period of vibrations and time of flight τ_f)[4,13,15]. The role of the time of flight from the photoabsorption site to a region of dissociation can be understood by comparing the RXS profiles for different isotopomers like HCl and DCl. These have the same potential surfaces and hence the corresponding RXS durations are the same for the same detuning Ω. However, the lighter isotopomer HCl has shorter time of flight than DCl, and reaches the dissociative region faster leading to a larger relative intensity of the AL resonance, see **Fig. 6**.

Simulations demonstrate the strong dependence of the spectral profile on the excitation energy- that is on the RXS duration time, with a narrow AL peak and a broad molecular background[4,8]. The center of gravity of the molecular background follows approximately the Raman law when the excitation energy is tuned out of the photoabsorption band[23,25], while the position of the AL resonance does not depend on the excitation energy[4,14] (7). The dispersion relation in the photoabsorption region strongly differs from the Raman law[23]. The numerical simulations also show this clearly, **Figs. 5** and **7**. When the excitation energy is tuned inside the photoabsorption band the dispersion relation for the center of gravity of the molecular pedestal shows non-Raman behavior[23], as observed recently by Piancastelli et al.[25]. The AL resonance is suppressed, up to depletion, for fast RXS corresponding to the excitation energies tuned out of the photoabsorption band (see **Figs. 5**, **7** and results of experimental measurements, **Fig. 8**).

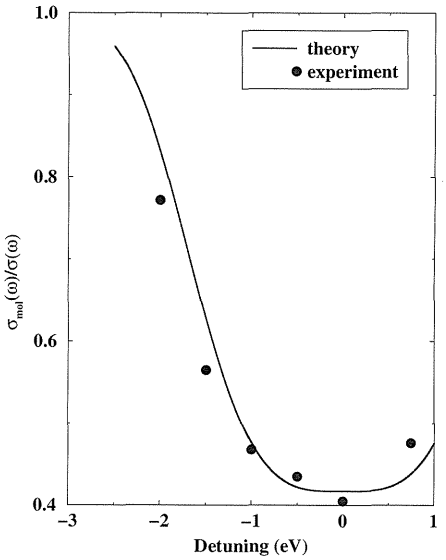

Figure 8. Comparison of the experimental and theoretical relative integral contribution of the molecular background[8].

4. Doppler Effects

The Doppler effect poses another dynamical problem in RXS, which, at first sight, appears to be quite exotic. However, in connection with the AL resonances[16,17,26], one can indeed expect large Doppler shifts due to a large release of kinetic energy, $\Delta E \simeq 1$-10 eV. A comparison of the different Doppler effects (**Fig. 9**) shows that the largest Doppler shift corresponds to RXS involving ejected Auger electrons in the spectral region with AL resonances. The reason of this is twofold; the large momentum of the Auger electrons p, and the large release velocity $v_A=(2\mu[\Omega-\{E-\omega_{cf}(\infty)\}]/m_A^2)^{1/2}$ of the dissociated atom.

It is interesting in this context to consider resonant Auger scattering from a homonuclear diatomic molecule A_2[17]. To take into account the indistinguishability of the two atoms one needs to sum the partial scattering amplitudes $F_{1,2}=f_{1,2}$ exp $(\pm iqR_f)$ for both atoms $F=F_1+F_2$, where $q=0.5p$ cos θ, R_f has the order of magnitude of equilibrium internuclear distance R[17]. The phase factors in $F_{1,2}$ are consequential: They lead to the generalized FC factors[17] (for bound-bound, bound-continuum, and continuum-continuum nuclear transitions) both in photoionization and in RXS. Due to the Doppler effect the partial scattering amplitudes f_1 and f_2 for atoms 1 and 2 are different[17,26]

$$f_{1,2}=\frac{(e\cdot d_{co})a}{v\pm D\cos\theta+i\Gamma},\quad D=pv_A,\quad v=E-\omega_{cf}(\infty). \tag{11}$$

Here θ is the angle between p and v_A. The case of nonradiative RXS from heteronuclear molecules, AB, is straightforward; only one term in $F=F_1+F_2$ must be kept.

Eq. (11) shows that the electron-ion coincidence signal changes drastically if the Auger electron energy E lies in the Doppler band $-pv_A<E-\omega_{cf}(\infty)<pv_A$. When Γ is smaller than the electron Doppler shift pv_A the photoions or neutral fragments of dissociation propagate in the narrow angular interval $\delta\theta\simeq\Gamma/pv_A$ close to the cone surface (**Fig. 10**) $\theta\simeq\theta_r$

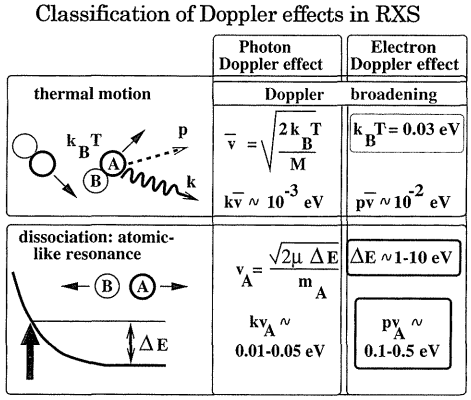

Figure 9. Classification of the Doppler effects. v_A is the speed of atom A in the dissociative region; $\bar{v}$ is the thermal velocity; k and p are momentums of the x-ray photon and Auger electron, respectively; ΔE is the energy released under dissociation. μ is the reduced mass.

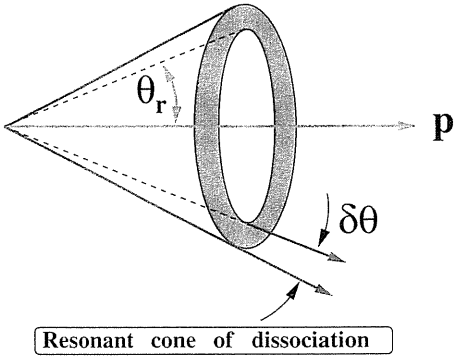

Figure 10. Resonant cone of dissociation.

$$\cos\theta_r=\frac{\omega_{cf}(\infty)-E}{pv_A},\quad \text{if}\ \left|\frac{\omega_{cf}(\infty)-E}{pv_A}\right|\le 1. \tag{12}$$

The appearance of the narrow resonant cone of dissociation with a "resonant" angle θ_r is an important result of the studied problem[17,26]. Expression for $\delta\theta$ clearly demonstrates the strong correlation between propagation directions of the Auger electron and the ion A^+.

The quantity of interest is the RXS cross section which is the sum of direct, $\sigma_1+\sigma_2$, and interference, σ_{int}, contributions

$$\sigma(E,\omega)=\sigma_1+\sigma_2+\sigma_{int}$$
$$=\sum_{f=g,u}(|f_1|^2+|f_2|^2+2\mathscr{R}e(f_1^*f_2e^{ikR_f\cos\theta})). \tag{13}$$

RXS measurements make it possible to distinguish "left" and "right" atoms in a homonuclear molecule A_2 molecule. We consider first the case when the interference can be neglected (for example when $|D\cos\theta|\gg\Gamma$). The scattering channels are then independent and the RXS cross section can be written as the sum of only direct contributions[17]

$$\sigma(E,\omega)\simeq|(\boldsymbol{e}\cdot\boldsymbol{d}_{co})a|^2\left(\frac{1}{(\nu-D\cos\theta)^2+\Gamma^2}\right.$$
$$\left.+\frac{1}{(\nu+D\cos\theta)^2+\Gamma^2}\right). \tag{14}$$

One can assume that the Auger electron is ejected along a molecular axis: ($\theta=0°$ or 180°). Two narrow Lorentzians (14) correspond to two opposite directions of the dissociating atoms. The large Doppler shift D destroys the coherence of the scattering channels $\sigma_{int}/\sigma(E,\omega)\sim\Gamma/pv_A\ll 1$ (**Fig. 11**). One can distinguish these channels since one now can select either of them through the "left propagating" and "right propagating" atoms A. It is possible to do so due to different "Doppler labels" (Doppler shifts): $-pv_A$ and pv_A. Thus the "Doppler labels" allow to select contributions to the RXS cross section from the core excited state with the core hole localized at a certain atom[17] (see also ref. 27).

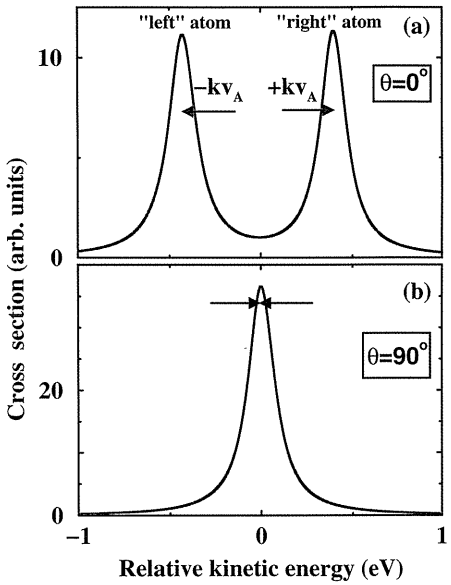

Figure 11. The dependence of the total RXS spectral profile $\sigma(E,\omega)$, on the relative kinetic energy $\nu=E-\omega_{cf}(\infty)$. $E=500$ eV, $\Omega=5$ eV, $\Gamma=0.09$ eV[17]. When $\theta=0°$ the "left" atom has red Doppler shift, while the "right" atom has blue Doppler shift. The equivalent atoms can be distinguished by the the Doppler labels $\pm kv_A$. One can not distinguish these atoms when $\theta=90°$ since in this case the Doppler shift is absent.

So the asymmetric measurements with the photoelectron detector at a certain side relative to the ionization region violate the symmetry of the partially oriented A^*A+AA^* system and select only one configuration, A^*A or AA^*, depending on the Auger electron energy and the direction of $\boldsymbol{p}$. The change from the entangled to disentangled state representations, with an accompanying destruction of the quantum correlation, is caused by the special measurement technique employed[26].

When the Auger electron is emitted perpendicular to the molecular axis the RXS profile collapses to a single Lorentzian since $\cos\theta=0$ and the Doppler shift is then exactly equal to zero (**Fig. 11**). Since the Doppler shift is absent when $\theta=90°$ one can not distinguish equivalent atoms in an A_2 molecule. In this case both scattering channels are strongly coherent and the interference term σ_{int} takes a maximal value (see **Fig. 11**).

Eqs. (13) and (14) correspond to oriented molecules. The measurement of the Doppler effect is possible also for a randomly oriented molecular target, as recently shown by Björneholm et al.[18]. Indeed, the ensemble of core excited molecules in a gas becomes partially oriented due to orientation selective core excitation ($\propto(\boldsymbol{e}\cdot\boldsymbol{d}_{co})^2$)[9,28,29].

Finally, we point to the striking role of the interchannel interference (13) in the narrowing of the RXS spectral profile[17] up to an HWHM of $\Delta\nu\simeq D/pR$ which thus does not depend on the lifetime broadening Γ, and can be smaller than the lifetime broadening, Γ, and the spectral function width, γ.

5. Dynamical Effects in Resonant X-Ray Scattering by Solids and Polymers

The concept of the RXS duration for time selection of the vibronic coupling in free molecules as well as special effects like the restoration of the selection rules[5,9,20,21] and the collapse effect[6,7,19,30] are also relevant for interpreting corresponding spectra of polymers and solids. Other effects in RXS from polymers[31,32], solids[3,33-46] and transition metal complexes[47-54] were reviewed recently. Just as for vibronic coupling in free molecules, one can anticipate that electron-phonon coupling is of primary importance to understand spectral shapes of RXS by polymers and solids. Effects due to vibronic coupling and momentum exchange between electrons and phonons are in general large because the degeneracy of the core shell leads to strong vibronic mixing of the core excited states. The breaking and restoration of the symmetry selection rules in gas-phase systems can then be understood as breaking and restoration of the momentum conservation rule in the the context of solids.

A main conclusion is that the electron-phonon interaction in x-ray Raman spectra is strongly dynamic, and that frequency detuning, and thereby a shortening of the duration of the scattering process, allows an active manipulation of the strength of the electron-phonon interaction. As is well established by now the momentum conservation law plays a very important role in the formation of the radiative RXS[19,40,55-58]

$$p=p'+p_{ph}+q+\Delta p+G. \tag{15}$$

Here p and p' are momenta of valence and conduction electrons, $q=k'-k$ is the change of the photon momentum k under a scattering, p_{ph} is momentum of the phonon, Δp is the change of the electron momentum due to scattering at the "heavy" core hole or at other electrons. The extra momentum G (a reciprocal lattice vector) is transferred to the crystal as a whole. We ignore here the momentum exchange between the core hole and the x-ray photons (see investigations of these effects in Ref. 58). To extract the main physics it is very useful to start out from eq. (8) which shows that in the case of fast RXS (large detuning) a direct transition from ground to final nuclear states takes place. In other words, the phonons "have no time" to disturb the electronic subsystem of the core excited states, for example, to exchange momenta with electrons. This results in a suppression of the electron-phonon interaction and a restoration of the electronic selection rules when the photon frequency is tuned below the photoabsorption edge[5,19,57,59]. The translational invariance which leads to the conservation law (15) is a main element of symmetry of crystalline solids, and the effect of the restoration of electronic selection rules means in particular that eq. (15) reduces to the conservation of electronic momentum under RXS[55,58]

$$p=p', \quad \tau_c \ll \tau_{vib} \simeq \omega_D^{-1} \tag{16}$$

with ω_D as the Debye frequency. This equation asserts that the RXS transitions are direct or vertical in the limit of fast RXS.

There are some striking consequences of the approximation (16): In a two-band system with semi-empty valence bands (like alkali metals) the direct RIXS transitions are forbidden when the excitation energy is smaller than $I_K+\Delta$, where I_K is the position of the photoabsorption edge[55,58], see **Fig. 12**. Thus the unusual effect prevails, that when the absorbed x-ray radiation creates a core hole ($\omega \geq I_K$), x-ray fluorescence is absent. The "vanished" RIXS intensity is transferred to the elastic cross section. Another example is given by RXS from one-band semi-empty systems, like π bands for linear polyenes: When the momentum conservation law (16) is valid the RIXS cross section is then exactly equal to zero[19,58], **Fig. 13**. The electron-phonon interaction has the effect to open the RIXS channel and to allow decay transitions from all occupied levels, while the momentum exchange between electrons and soft x-ray photons allows emission only from the highest occupied levels[19,58], **Fig. 14**. We note that all occupied molecular orbitals (all valence bands) become active for RIXS in the hard x-ray region with large

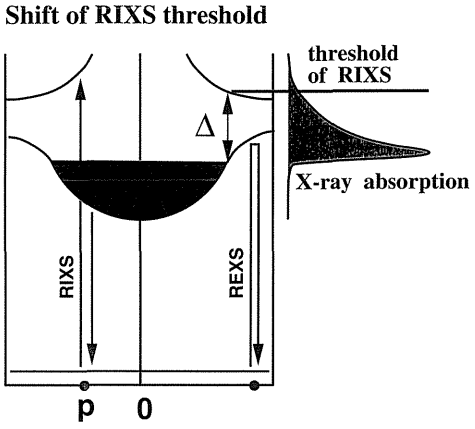

Figure 12. Shift of inelastic RXS (RIXS) threshold due to momentum conservation law (16).

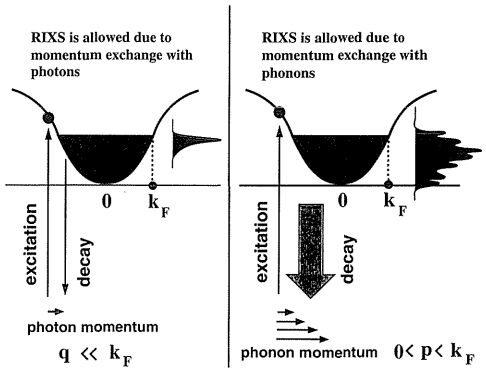

Figure 13. Formation of the RIXS profile due to momentum exchange with photons and phonons. Left panel: Small photon momenta open the inelastic channels in the narrow region near the Fermi level. Right panel: Large phonon momenta open the inelastic channels for all occupied levels[19,58].

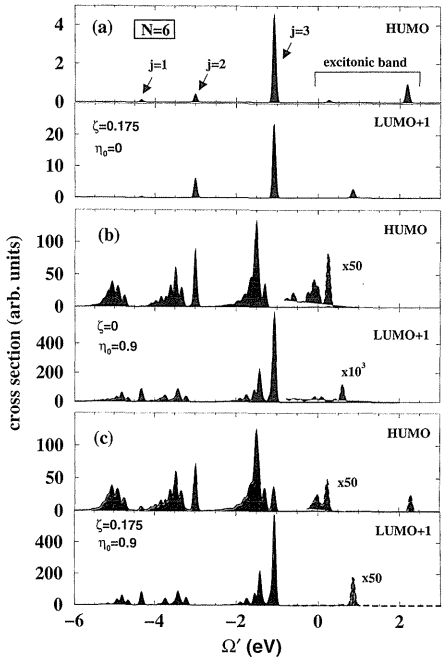

Figure 14. The RIXS cross section of a $N=6$ polyene versus the momentum exchange of valence electrons with x-ray photons and phonons[19]. Here N is the number of carbons. (a) accounting only for momentum exchange between electrons and photons; (b) accounting only for momentum exchange between electron and phonons; (c) accounting for momentum exchange of electron with both photons and phonons. The cross section is decreased by 10^3 times. $\Gamma=0.09$ eV, $\gamma=0.05$ eV, $I_K=290$ eV, $\omega_o=0.5$ eV. The abbreviations HUMO and LUMO+1 mean the core excitation ($\Omega=w_\nu$) to the highest unoccupied MO ψ_ν ($\nu=6$) and to the MO with $\nu=5$, respectively. The arrows in panel (a) mark the positions of the zero-phonon lines for the decay transitions from occupied MO ψ_j with $j=1, 2, 3$. The dashed lines in the panels (b) and (c) show the excitonic bands. The energy corresponding to molecular Orbital ψ_j *is* $\varepsilon_j=\varepsilon_F+w_j$, ε_F is the Fermi energy. $\Omega=\omega-(I_K+\varepsilon_F)$ and $\Omega'=\omega'-(I_K+\varepsilon_F)$ are detunings of initial and final x-ray photons.

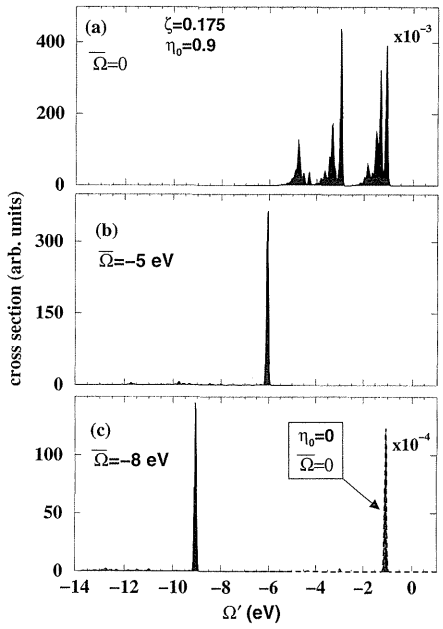

Figure 15. Collapse of vibrational structure in RIXS of a $N=6$ polyene due to the detuning of incident x-ray radiation from the absorption band[19]. The potential surfaces of initial and final states are the same. The momentum exchange with x-ray photon is taken into account. The detuning of incident radiation from the LUMO ($\nu=4$) is defined as $\bar{\Omega}=\Omega-w_{M+1}$, $M=3$. (a) The resonant excitation of the LUMO ($\Omega=w_{M+1}$) leads to the vibrational broadening of the RIXS profile (the cross section is decreased by 10^3 times). Panels (b) and (c) show the collapse effect corresponding to a detuning of incident radiation below the LUMO with $\bar{\Omega}=-5$ eV and $\bar{\Omega}=-8$ eV, respectively. The dashed line in panel (c) shows the RIXS cross section for resonant excitation of the LUMO and without electron-phonon interaction ($\bar{\Omega}=0$). The value of the VC parameter is the same, $\eta_o=0.9$, except for the RIXS profile shown by dashed line with $\eta_o=0$[19]. All other parameters are the same as for Fig. 14.

photon momenta[19,58].

Fig. 15 shows two effects: Collapse of vibrational structure[6,7,19] and restoration of electronic selection rules[5,19-21]. When the excitation energy is tuned to resonance with the first photoabsorption line (**Fig. 15**a) all three electron-phonon bands are active in RIXS due to strong electron-phonon interaction with large phonon momenta. **Figs. 15**b, c correspond to fast RIXS with strong quenching of electron-phonon interaction. We see here a single line which is allowed only due to the photon momentum (small photon momentum opens only emission transitions from the highest occupied MO close to the Fermi level). This is a clear manifestation of the restoration of electronic selection rules (here, the restoration of the momentum conservation law (16)). It is not hard to realize also a collapse of the vibrational structure: **Fig. 15**b, c. show clearly only a single resonance without any vibrational structure.

The collapse effect is not complete in the case with different interatomic potential surfaces of the ground and final states[19]. The RXS profile collapses strictly to a single resonance for the elastic band since the potential surfaces of the ground and final states are the same in such a case. The collapse effect will in general be difficult to observe in solids due to the nonparallel valence and conduction bands, except maybe at the spectral region near the singularities of the joint density of states[19]. The complete collapse in RXS from solids thus takes place in the spectral region with parallel conduction and valence bands.

So we see that symmetry restoration and collapse effects are caused by the interplay of two different time scales in RXS; the duration of scattering and the period of vibration. Selection rules may also break down if vibronic coupling mixes final electronic states of different symmetry. However, for π systems it can be shown that this final-state symmetry breaking is also suppressed upon detuning the excitation frequency[19], and also in this case, detuning makes the RIXS cross section close to zero.

These dynamic features are dependent on both the width and the carrier frequency of the exciting radiation. Each RXS electron-phonon band consists of a zero-phonon line and red and blue phonon sidebands. The zero-phonon line has specific selection rules for narrow band excitation[19]. For

sufficiently small sample molecules (or long wavelengths) the selection rules for the partial cross sections are maintained since the dipole approximation over the molecular size can be used[19].

The problem of core hole localization in RXS from solids deserves a brief comment. It is easy to see that the electron-phonon interaction mixes the electronic Bloch functions of the core shell with different momenta. This results in a lowering of symmetry of the core excited states up to the complete localization of the core hole at one of the atoms. One manifestation of this is the breakdown of the momentum conservation law. We have seen that the violation of this law and hence the core hole localization is strongest if the excitation frequency is tuned in the region of strong photoabsorption. However, when the frequency is detuned below a photoabsorption edge the momentum conservation law, the selection rules and the symmetry of the electronic subsystem are restored. We conclude that the shortening of the RXS duration (increase of detuning frequency) in a certain sense leads to a delocalization of the core hole (see also refs. 60, 61).

Acknowledgements

One of the authors (H. Å) wishes to convey many thanks to Prof. Nobuhiro Kosugi at IMS in Okazaki for organizing a most pleasant and scientifically rewarding 3-month visit in Japan.

References

1) T. Åberg and B. Crasemann. In G. Materlik, C. J. Sparks and K. Fischer: editors, *Resonant Anomalous X-Ray Scattering. Theory and Applications*, page 431. North-Holland, Amsterdam, 1994.
2) F. Gel'mukhanov and H. Ågren: *Phys. Rep.*, **00**, 000 (1999).
3) A. Kotani: *J. Phys. (France)*, IV, 7: C2-1, 1997.
4) F. Gel'mukhanov and H. Ågren: *Phys. Rev.* **A54**, 379 (1996).
5) P. Skytt, P. Glans, J.-H. Guo, K. Gunnelin, J. Nordgren, F. Gel'mukhanov, A. Cesar and H. Ågren: *Phys. Rev. Lett.* **77**, 5035 (1996).
6) F. Gel'mukhanov, T. Privalov and H. Ågren: *Phys. Rev.* **A56**, 256 (1997).
7) S. Sundin, F. Gel'mukhanov, H. Ågren, S. J. Osborne, A. Kikas, O. Björneholm, A. Ausmees and S. Svensson: *Phys. Rev. Lett.* **79**, 1451 (1997).
8) O. Björneholm, S. Sundin, S. Svensson, R. R. T. Marinho, A. Naves de Brito, F. Gel'mukhanov and H. Ågren: *Phys. Rev. Lett.* **79**, 3150 (1997).
9) J. Nordgren: *J. Phys. (France)*, IV, 7: C2-9, 1997.
10) S. Tanaka, Y. Kayanuma and K. Ueda: *Phys. Rev.* **A57**, 3437 (1998).
11) Z. Gortel, R. Teshima and D. Mentzel: *Phys. Rev.* **A58**, 1225 (1998).
12) Z. Gortel and D. Mentzel: *Phys. Rev.* **A58**, 3699 (1998).
13) F. Gel'mukhanov, P. Salek, T. Privalov and H. Ågren: *Phys. Rev.* **A59**, 380 (1999).
14) E. Kukk, H. Aksela, S. Aksela, F. Gel'mukhanov, H. Ågren and S. Svensson: *Phys. Rev. Lett.* **76**, 3100 (1996).
15) P. Salek, F. Gel'mukhanov and H. Ågren: *Phys. Rev.* **A59**, 1147 (1999).
16) S. Sundin: "Photoelectron Spectroscopy in the Vicinity of a Core-Ionization Threshold", Ph.D. Thesis, Uppsala University, 1998.
17) F. Gel'mukhanov, H. Ågren and P. Salek: Phys. Rev. **A57**, 2511 (1998).
18) O. Björneholm et al.: Phys. Rev. Lett. (submitted).
19) T. Privalov, F. Gel'mukhanov and H. Ågren: *Phys. Rev.* **B59**, 000 (1999).
20) A. Cesar, F. Gel'mukhanov, Y. Luo, H. Ågren, P. Skytt, P. Glans, J.-H. Guo, K. Gunnelin and J. Nordgren: *J. Chem. Phys.* **106**, 3439 (1997).
21) F. Gel'mukhanov, H. Ågren and T. Privalov: *JETP* **85**, 20 (1997).
22) P. Morin and I. Nenner: *Phys. Rev. Lett.* **56**, 1913 (1996).
23) F. Gel'mukhanov and H. Ågren: *Phys. Rev.* **A54**, 3960 (1996).
24) F. Gel'mukhanov and H. Ågren: Phys. Rev. **A49**, 4378 (1994).
25) M. N. Piancastelli, B. Kempgens, U. Hergenhahn, A. Kivimäki, K. Maier, A. Rüdel and A. M. Bradshaw: *Phys. Rev.* **A59**, 1336 (1999).
26) F. Gel'mukhanov and H. Ågren: *Pis'ma Zh. Eksp. Teor. Fiz.* **67**, 1005 (1998). [JETP Lett. **67**, 1064 (1998)].
27) K. Ueda, Y. Shimizu, H. Chiba, M. Okunishi, K. Ohmori, J. B. West, Y. Sato, T. Hayaishi, H. Nakamatsu and T. Mukoyama: *Phys. Rev.* **A79**, 3371 (1997).
28) F. Gel'mukhanov and L. N. Mazalov: Opt. Spectrosk. **42**, 659 (1977) [Opt. Spectrosc. (USSSR) **42**, 371 (1977)].
29) E. Shigemasa, J. Adachi, K. Soejima, N. Watanabe, A. Yagishita and N. A. Cherepkov: *Phys. Rev. Lett.* **80**, 1622 (1998).
30) S. Svensson and A. Ausmees: *Appl. Phys. A: Mater. Sci. Process.* **65**, 107 (1997).
31) J.-H. Guo, M. Magnuson, C. Såthe, J. Nordgren, L. Yang, Y. Luo, H. Ågren, K. Z. Xing, N. Johansson, W. R. Salaneck and W. J. Feast: *J. Chem. Phys.* **108**, 5990 (1998).
32) M. Magnuson, L. Yang, J.-H. Guo, C. Såthe, A. Agui, J. Nordgren, Y. Luo, H. Ågren, N. Johansson, W. R. Salaneck, L. E. Horsburgh and A. P. Monkman: *Chem. Phys.* **237**, 295 (1998).
33) T. Kashiwakura, H. Arai, N. Kozuka, K. Odagawa, T. Yokohama, A. Kamata and S. Nakai: *J. Electron Spectrosc. Rel. Phen.* **79**, 207 (1996).
34) K. Yoshii, Y. Baba and T. A. Sasaki: *J. Electron Spectrosc. Rel. Phen.* **79**, 215 (1996).
35) N. Mårtensson, M. Weinelt, O. Karis, M. Magnuson, N. WassdahL, A. Nilsson, J. Stöhr and M. Samant: *Appl. Phys. A: Mater. Sci. Process.* **65**, 159 (1997).
36) Y. Iwasawa: *J. Phys. (France)*, IV, 7: C2-67, 1997.
37) P. P. Kane: *Radiat. Phys. Chem.* **50**, 31 (1997).
38) M. Weinelt, A. Nilsson, M. Magnuson, T. Wiell, N. Wassdahl, O. Karis, A. Föhlisch, N. Mårtensson, J. Stöhr and M. Samant: *Phys. Rev. Lett.* **78**, 967 (1997).
39) S. Tanaka and Y. Kayanuma: *J. Phys. (France)*, IV, 7: C2-103, 1997.
40) T. Minami and K. Nasu: *Phys. Rev.* **B57**, 12084 (1998).
41) A. Agui, S. Shin, M. Fujisawa, Y. Tezuka, T. Ishii, Y. Muramatsu, O. Mishima and K. Era: *Phys. Rev.* **B55**, 2073 (1997).
42) A. Agui, S. Shin, M. Fujisawa, Y. Tezuka, T. Ishii, O. Mishima, K. Era, E. Shigemasa and A. Yagishita: *J. Electron Spectrosc. Rel. Phen.* **79**, 191 (1996).
43) J. J. Jia, T. A. Calcott, E. L. Shirley, J. A. Carlisle, L. J. Terminello, A. Asfaw, D. L. Ederer, F. J. Himpsel and R. C. C. Perera: *Phys. Rev. Lett.* **76**, 4054 (1996).
44) Y. Tezuka, S. Shin, A. Agui, M. Fujisawa and T. Ishii: *Phys. Soc. Jpn* **65**, 213 (1996).

45) Y. Tezuka, S. Shin, A. Agui, M. Fujisawa, T. Ishii and A. Yagishita: *J. Electron Spectrosc. Rel. Phen.* **79**, 195 (1996).
46) J. J. Jia, T. A. Calcott, A. Asfaw, J. A. Carlisle, L. J. Terminello, D. L. Ederer, F. J. Himpsel and R. C. C. Perera: *Phys. Rev.* **B52**, 4904 (1995).
47) Y. Takata, M. Nakamura and N. Kosugi: *Chem. Phys. Lett.* **287**, 35 (1998).
48) Y. Takata, T. Hatsui and N. Kosugi: *J. Electron Spectrosc. Rel. Phen.* **88**, 235 (1998).
49) Y. Takata, M. Nakamura and N. Kosugi: *J. Electron Spectrosc. Rel. Phen.* **93**, 109 (1998).
50) K. Okada and A. Kotani: *J. Electron Spectrosc. Rel. Phen.* **88**, 55 (1998).
51) K. G. Nath, Y. Ufuktepe, S. Kimura, T. Kinoshita, H. Kumigashira, T. Takahashi, T. Matsumura, T. Suzuki, H. Ogasawara and A. Kotani: *J. Electron Spectrosc. Rel. Phen.* **88**, 369 (1998).
52) T. Kinoshita, Y. Ufuktepe, K. G. Nath, S. Kimura, H. Kumigashira, T. Takahashi, T. Matsumura, T. Suzuki, H. Ogasawara and A. Kotani: *J. Electron Spectrosc. Rel. Phen.* **88**, 255 (1998).
53) K. Ogasawara, A. Kotani, J. P. Hill, C. C. Kao, W. A. L. Caliebe, M. Matsubara, A. Kotani, J. L. Peng and R. L. Greene: *Phys. Rev. Lett.* **80**, 4967 (1998).
54) K. Ogasawara and A. Kotani: *J. Electron Spectrosc. Rel. Phen.* **88**, 261 (1998).
55) F. Gel'mukhanov, L. N. Mazalov and N. A. Shklyaeva: Zh. Eksp. Teor. Fiz. **71**, 960 (1976) [Sov. Phys. JETP **44**, 504 (1977)].
56) J. A. Carlisle, E. L. Shirley, E. A. Hudson, L. J. Terminello, T. A. Callcott, J. J. Jia, D. L. Ederer, R. C. C. Perera and F. J. Himpsel: *Phys. Rev. Lett.* **74**, 1234 (1995).
57) S. Shin, A. Agui, M. Watanabe, M. Fujisawa, Y. Tezuka and T. Ishii: *Phys. Rev.* **B53**, 15660 (1996).
58) F. Gel'mukhanov and H. Ågren: *Phys. Rev.* **B57**, 2780 (1998).
59) P. Skytt, J.-H. Guo, N. Wassdahl, J. Nordgren, Y. Luo and H. Ågren: *Phys. Rev.* **A52**, 3572 (1995).
60) F. Gel'mukhanov and H. Ågren: *J. Electron Spectrosc. Rel. Phen.* **93**, 31 (1998).
61) F. Gel'mukhanov and H. Ågren: *Phys. Rev. Lett.* **82**, 666 (1999).